

UDC 541.11:661.183

DOI: 10.15372/CSD20170613

# Packing Design of Carbon Layers in Kemerit Highly Porous Carbon Material

D. G. YAKUBIK<sup>1</sup>, A. A. MULYUKOVA<sup>2</sup>, CH. N. BARNAKOV<sup>2</sup><sup>1</sup>*Kemerovo State University,  
Kemerovo, Russia**E-mail: den@kemsu.ru*<sup>2</sup>*Institute of Coal Chemistry and Material Science, Federal Research Center of Coal and Coal Chemistry,  
Siberian Branch. Russian Academy of Sciences, Kemerovo, Russia*

(Received October 01, 2017)

## Abstract

The paper considers the structural characteristics of a promising mesoporous material Kemerit to develop ionistors. Location model of carbon layers is proposed. According to it, three-dimensional ordered nanocrystalline domains are a random overlay of strongly peaked graphene planes. Modelling of the resulting structures is carried out by the molecular dynamics method. The findings qualitatively coincide with the XPA and Raman spectroscopy data.

**Keywords:** highly porous carbon materials, molecular dynamics, nanocrystalline domains, structure

## INTRODUCTION

Currently, porous carbon materials (PCM) have found broad applications as hemosorbents [1], catalyst carriers [2], electrode materials for energy storage devices [3], and for heavy metal extraction [4]. An important aspect of improving the properties of highly porous materials is the study of the regularities of the generation of their structural and textural parameters that affect sorptive and electrochemical properties. A promising approach for understanding the texture generation process between the synthesis conditions and structures of the resulting carbon materials is the synthesis of PCM from individual aromatic compounds. Carbonization study of substances with the known composition and structure is likely

to allow further revealing the generation mechanism of PCM texture and synthesizing carbon materials with predetermined properties.

A group of highly porous carbon materials with a general name of Kemerit synthesized in the Federal Research Center of Coal and Coal Chemistry (FRC CCC SB RAS) are such materials [5–8]. Microporous PCM with a high specific surface area are generated during carbonization of oxygen- and nitrogen-containing organic compounds (individual and in a mixture), while mesoporous PCM – during the addition of furfural to the reaction mixture.

The present work considers the structural characteristics of mesoporous carbon materials synthesized from a mixture of hydroquinone and furfural (Kem-5 and Kem-6) and of phenol and furfural (Kem-7 and Kem-8).

TABLE 1

Conditions for synthesis of mesoporous carbon materials (MPC)

Samples	Precursor ratio, mol/mol	Synthesis conditions
Kem-5	Hydroquinone + furfural (1 : 2)	$T = 700\text{ }^{\circ}\text{C}$ , $t = 60\text{ min}$
Kem-6	Same (1 : 1)	$T = 700\text{ }^{\circ}\text{C}$ , $t = 60\text{ min}$
Kem-7	Phenol + furfural (1 : 2)	$T = 900\text{ }^{\circ}\text{C}$ , $t = 10\text{ min}$
Kem-8	Same (1 : 1)	$T = 900\text{ }^{\circ}\text{C}$ , $t = 10\text{ min}$

Note.  $T$  – carbonization temperature,  $t$  – carbonization time.

## EXPERIMENTAL

Synthesis of PCM with a developed surface was carried out in two steps. In the beginning, starting materials (precursors) were mixed with an equimolar mixture of sodium and potassium hydroxides in a mass ratio of 1 : 5; the resulting mixture was exposed to melting at  $\sim 250\text{ }^{\circ}\text{C}$  for 3 h. At the second step, the melt was carbonized in the air at  $700\text{--}900\text{ }^{\circ}\text{C}$  for a certain time (see Table 1). The resulting carbonizate was rinsed with water until neutral medium and dried to constant mass at  $105\text{ }^{\circ}\text{C}$  [5].

Recording X-ray diffraction patterns was carried out on an HZG-4 diffractometer with  $\text{CuK}_{\alpha}$  radiation.

Raman spectra were produced on a Raman Horiba Jobin Yvon LabRAM HR800 spectrometer.

A helium-neon laser with the main line of pumping of  $633\text{ nm}$  was used as a light source.

## RESULTS AND DISCUSSION

### X-ray phase analysis

Reflexes of Kemerit porous carbon material are strongly broadened, which points to a high degree of amorphism of synthesized carbon materials (Fig. 1). A reflex of 002 is shifted towards small angles ( $\sim 22.5^{\circ}$ ) relative to a reflex of 002 ( $\sim 26.5^{\circ}$ ) of ideal graphite, which attests to interplanar spacing increase in PCM ( $3.95\text{ \AA}$ ) by 15–18%. In addition, a low expressed peak near  $14^{\circ}$  that attests to the presence of structures with an interplanar spacing of  $6.61\text{ \AA}$  can be seen in X-ray diffraction patterns.

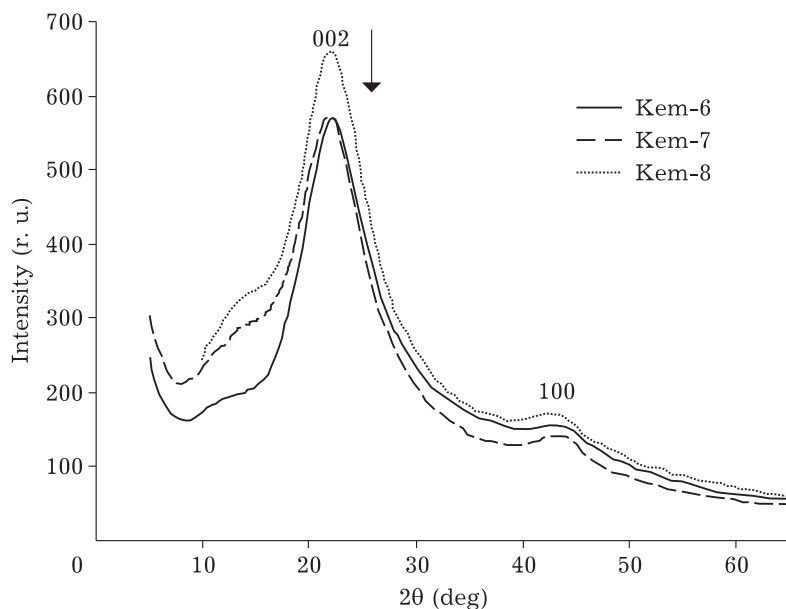


Fig. 1. X-ray diffraction patterns of three PCM samples (Kem-6, Kem-7, and Kem-8) with a developed mesoporosity.

TABLE 2

Number of layers ( $N_1$ ), interlayer distance ( $d_{002}$ ), and the crystallite thickness ( $D$ ) of multilayer graphene [8, with changes]

$N_1$	$d_{002}$ , Å	$D$ , Å
3	3.664	7.327
4	3.474	40.422
5	3.426	13.704
6	3.420	17.100
7	3.414	20.484

Parameters characterizing spatially homogeneous regions were assessed according to a value of reflexes of 002 and 100 [8]. The average size of ordered crystallites is 1.0–1.5 nm and 1.0–1.2 nm along the  $a$  and  $c$  axes, respectively (3–4 graphene layers).

Alternative assessment of the number of layers in the domain may be carried out according to the interplanar spacing value along an axis with  $d_{002}$ . Paper [9] gives the following data regarding the interrelationship between  $d_{002}$  and the number of layers along the axis  $N_1$  (Table 2).

The interrelationship between  $N_1$  and  $d_{002}$  may be approximated by the following formula:  $N_1 = 0.694 \ln((d_{002} - 3.414)/18.81)$

Using an experimental value of  $d_{002}$  (3.95 Å) for this formula the average number of layers of 2.5 (two- and three-layer packing) may be obtained.

### Raman spectroscopy

Raman spectra of the studied PCM samples contain two strong lines in the 1000–1800  $\text{cm}^{-1}$  range (Fig. 2). The G line (1580–1600  $\text{cm}^{-1}$ ) corresponds to the allowed  $E_{2g}$  vibrations of hexagonal graphite lattice. The significant intensity of the D line (1310–1340  $\text{cm}^{-1}$ ) corresponding to the  $A_{1g}$  vibrational mode forbidden by the selection rules for ideal graphite attests to the presence of a large number of structural defects. Both lines refer to the  $sp^2$ -hybridised carbon [10]. In addition, D line asymmetry demonstrates the presence of a weak line in the 1000–1100  $\text{cm}^{-1}$  range corresponding to the scattering by the vibrations of  $sp^3$ -hybridized carbon (T line) [10].

As demonstrated in [11], the relationship between the ratios of the intensities of the D and G lines and the average crystallite size along the  $a$  axis is defined by the formula:

$$L_a = (2.4 \cdot 10^{-10}) \lambda_1^4 (I_D/I_G)^{-1}$$

where  $\lambda_1$  is the laser radiation wave length. Table 3 gives calculation results according to this formula. A similar assessment of crystallite sizes along the  $c$  axis [12] failed because of the diffusive nature of the D' and G' peaks in the 2700–2900  $\text{cm}^{-1}$  range (see Fig. 2).

As can be seen from the data of Table 3, the average crystallite size along the  $a$  axis

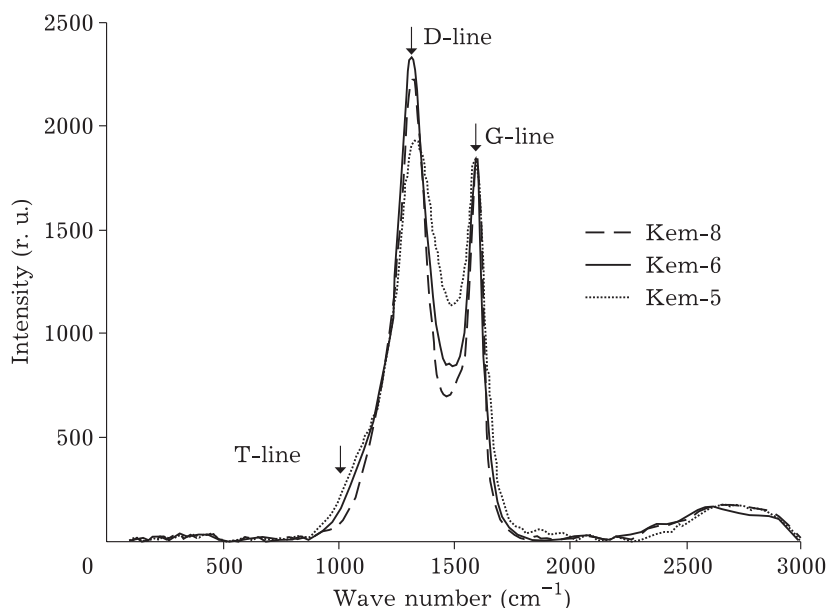


Fig. 2. Raman spectra of PCM samples (Kem-5, Kem-6, and Kem-8) of mesoporous carbon materials.

TABLE 3

Parameters of Raman spectra of Kemerit porous carbon materials

Parameters	Kem-5	Kem-6	Kem-8
Maximum of D-band $I_D$ , $\text{cm}^{-1}$	1325	1312	1339
Maximum of G-band $I_G$ , $\text{cm}^{-1}$	1597	1597	1579
D-band intensity ( $I_D$ ), r. u.	2115.75	2127.66	1783.28
G-band intensity ( $I_G$ ), r. u.	1835.22	1837.00	1806.64
$I_D/I_G$ ratio	1.15	1.16	0.99
Crystallite size along the $a$ axis ( $L_a$ ), nm	33.5	33.4	38.8

determined according to Raman spectroscopy data by more than an order of magnitude exceeds the dimension defined according to XPA data. To explain so substantial difference in assessments, it is worth noting that in Raman spectra, the ratio of the number of atoms in the ideal lattice to that in crystallite surface and near defects is determined, while in the XPA method – the number of atomic rows along the layer. It can be suggested that the ratio of peaks ( $I_D/I_G$ ) will be the same for graphene layers with an identical fraction of atoms in the ideal lattice ( $N_{\text{int}}/N_0$ ). Then, strongly indented graphene sheet with typical ordered linear size of 1.2–1.5 nm will have the same fraction of internal atoms (and, accordingly, the ratio of  $I_D/I_G$  peaks) as a continuous graphene sheet with internal defects with sizes of 30–40 nm.

### Model for the packing of carbon layers

Summarizing the above, one can put forward a model for the packing of carbon layers in Kemerit porous carbon material based on the following assumptions:

Graphene layers have no internal defects.

The size of ordered fragments along the  $a$  axis is 1.2–1.5 nm.

The ratio of atoms in the surface and inside the graphene sheet is found within 0.35–0.40.

Single graphene sheets are strongly indented (Fig. 3).

Graphene sheets are located almost in parallel, but they are chaotically turned relative to each other.

As a result of this, coincidences of ordered fragments forming two-, three-, and, rarely, four-domains are relatively rare.

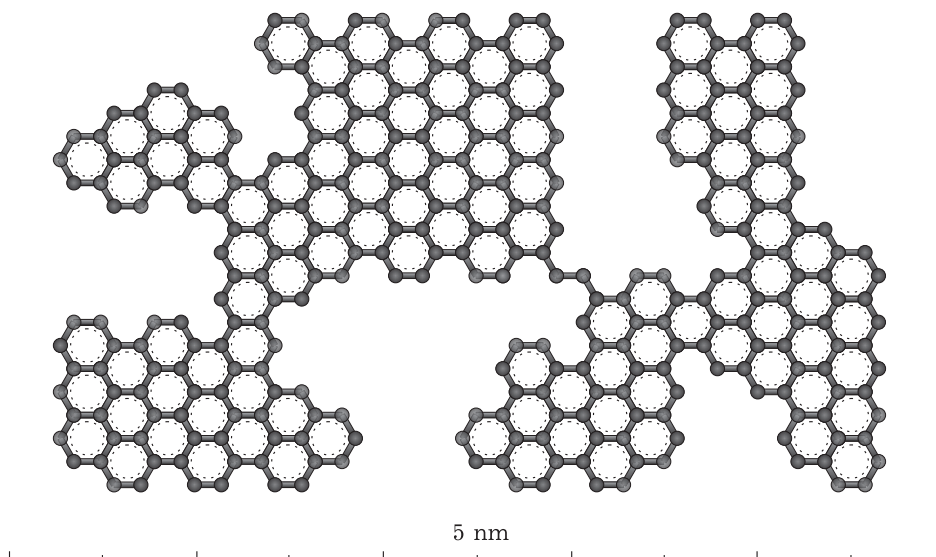


Fig. 3. Single strongly indented graphene sheet.

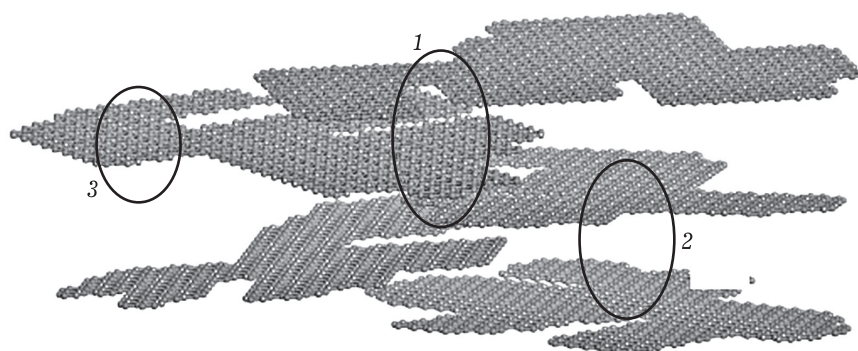


Fig. 4. Model ensemble for graphene sheets: 1 – overlap region of three ordered fragments ( $\sim 4 \text{ \AA}$ ), 2 – overlapping of two layers with the increased distance ( $\sim 6 \text{ \AA}$ ), 3 – mismatched fragments of graphene planes.

The fraction of coinciding ordered fragments are separated by an empty space of the intermediate layer, forming structures with the increased interatomic distance.

The PCM structure is constructed from random overlaying of these sheets, in most cases almost parallel. Different options are possible. Carbon fragments of different layers may find themselves over one another, then, 3–4 layer areas with an interlayer distance of about  $4 \text{ \AA}$  are produced. They appear in XRD spectra at  $2\theta = 22^\circ$ . They can alternate through the layer, then, the interlayer distance is about  $6.6 \text{ \AA}$ , producing the X-ray peak at  $2\theta = 14^\circ$ , and may generally not coincide giving the voids (Fig. 4).

To verify model adequacy molecular dynamic modeling of the five-layer fragment given in Fig. 4 was carried out. The simulation was performed within the canonical NVT ensemble using the Noze–Hoover thermostat; the constant of the thermostat was 1; the temperature was  $300 \text{ K}$ ; the interaction between atoms was described by Dreiding force field. The integration of Newton's equations was carried out by the Verlet method, the relaxation time of  $1\text{--}5 \text{ ps}$ , the calculation time of  $5\text{--}20 \text{ ps}$ , the time step of  $1\text{--}2 \text{ ps}$ . The calculations were performed in the program GULP [13] on a computing cluster of the Kemerovo State University. For the optimized structure, the scattering intensity of X-rays was calculated using the Debyer software according to the Debye formula [14]. Simulation results qualitatively correspond to experimental data; the peaks near  $2\theta = 14, 22, 42^\circ$  appear.

However, their intensities are very different from the experimental ones, which suggests the need for modeling of longer fragments.

## CONCLUSIONS

Assessment of ordered fragments along the  $a$  axis differs by more than an order of magnitude according to XPA and Raman spectroscopy ( $1.2\text{--}1.5 \text{ nm}$  and  $33\text{--}38 \text{ nm}$ , respectively).

A model of the packing of carbon layers in Kemerit porous carbon materials, according to which strongly indented graphene layers are located almost in parallel, however, they are chaotically turned relative to each other.

3. A molecular dynamic simulation of the five-layer packing was carried out; the calculated profile of scattering of X-rays qualitatively corresponds to experimental.

## REFERENCES

- 1 Mikhalovsky S. V., Nikolaev V. G., *Activated Carbon Surfaces in Environmental Remediation*. 2006. Vol. 7. P. 529–561.
- 2 Ismagilov Z. H., Kerzhentsev M. A., Shikina N. V., Lisitsyn A. S., Okhlopko L. B., Barnakov Ch. N., Masao Sakashita, Takashi Iijima, Kenichiro Tadokoro, *Catal. Today*. 2005. Vol. 102–103. P. 58–66.
- 3 Mateishina Yu. G., Ulikhin A. S., Samarov A. V., Barnakov Ch. N., Uvarov N. F., *Solid State Ionics*. 2013. Vol. 251. P. 59–61
- 4 Shavinskii B. M., Levchenko L. M., Mit'kin V. N., Galitskii A. A., Golovizina T. S., *Khimiya Ust. Razv.* 2008. Vol. 16, No. 4. P. 449–454.
- 5 RF Pat. No. 2206394, 2003.

- 6 Barnakov Ch. N., Kozlov A. P., *Zhurn. Neorgan. Khimii*. 2009. No. 12. P. 1962–1966.
- 7 RF Pat. No. 2307069, 2007.
- 8 Barnakov Ch. N., Samarov A. A., Shikina N. V., Yakubik D. G., *Khimiya Ust. Razv.* 2015. Vol. 23, No. 2. P. 219–223.
- 9 Seung Hun Huh, *Carbon*. 2014. Vol. 78. P. 617–621.
- 10 Ferrari A. C., Robertson J., *Phys. Rev. B* 64, 075414.
- 11 Pimenta M. A., Dresselhaus G., Dresselhaus M. S., Cancado I. G., Jorio A., Saito E., *Phys. Chem. Chem. Phys.* 2007. Vol. 9. P. 1276–1291.
- 12 Cancado L. G., Takai K., Enoki T., Endo M., Kim Y. A., Mizusaki H., Speziali N. L., Jorio A., Pimenta M. A., *Carbon*. 2008. Vol. 46. P. 272–275.
- 13 Gale J. D., Rohl A. L., *Mol. Simul.* 2003. Vol. 29. P. 291–341.
- 14 [Electronic resource]: URL: <http://github.com/wojdyr/debyer> (accessed 01.10.17).